Cold Regions Science and Technology 210 (2023) 103819

Contents lists available at ScienceDirect

Cold Regions Science and Technology

journal homepage: www.elsevier.com/locate/coldregions

An evaluation of GPR monitoring methods on varying river ice conditions: A case study in Alaska

Elizabeth Richards [a], Svetlana Stuefer [b,*], Rodrigo Correa Rangel [c], Christopher Maio [d], Nathan Belz [e], Ronald Daanen [f]

[a] U. S. Geological Survey Alaska Science Center, 3400 Shell Street, Fairbanks, AK 99701, United States of America
[b] University of Alaska Fairbanks, 1764 Tanana Loop, Suite 362, Fairbanks, AK 99775-5860, United States of America
[c] Department of Geology and Geophysics, University of Wyoming, 1000 E. University Ave., Laramie, WY 82071, United States of America
[d] University of Alaska Fairbanks, PO Box 755780, Fairbanks, AK 99775, United States of America
[e] University of Alaska Fairbanks, 1764 Tanana Loop, ELIF 128, Fairbanks, AK 99775-5860, United States of America
[f] Alaska Division of Geological & Geophysical Surveys, 3354 College Road, Fairbanks, AK, 99709, United States of America

ARTICLE INFO

Keywords:
Alaska
River ice
Ice thickness
GPR
Ice road

ABSTRACT

Ice roads and bridges across rivers, estuaries, and lakes are common transportation routes during winter in regions of the circumpolar north. Ice thickness, hydraulic hazards, climate variability and associated warmer air temperatures have always raised safety concerns and uncertainty among those who travel floating ice road routes. One way to address safety concerns is to monitor ice conditions throughout the season. We tested ground penetrating radar (GPR) for its ability and accuracy in measuring floating ice thickness under three specific conditions: 1) presence of snow cover and overflow, 2) presence of snow cover, and 3) bare ice, all common to Interior Alaska rivers. In addition, frazil ice was evaluated for its ability to interfere with the GPR measurement of ice thickness. We collected manual ice measurements and GPR cross-sectional transects over 2 years on the Tanana River near Fairbanks, Alaska, and for 1 year on the Yukon River near Tanana, Alaska. Ground truth measurements were compared with ice thickness calculated from an average velocity model created using GPR data. The error was as low as 2.3–6.4% on the Yukon River (Condition 3) and 4.6–9.5% on the Tanana River (Conditions 1 and 2), with the highest errors caused by overflow conditions. We determined that certain environmental conditions such as snow cover and overflow change the validity of an average velocity model for ice thickness identification using GPR, while frazil ice accumulation does not have a detectable effect on the strength of radar reflection at the ice-water interface with the frequencies tested. Ground penetrating radar is a powerful tool for measuring river ice thickness, yet further research is needed to advance the ability of rural communities to monitor ice thickness using fewer time-intensive manual measurements to determine the safety of ice cover on transportation routes.

1. Introduction

Seasonal ice cover has a significant effect on the hydrology and environment of northern rivers, changing river flow regime and local ecology during winter months. River ice in Interior Alaska has the potential to be both beneficial and detrimental: it provides winter transportation routes for remote rural residents and allows for movement of heavy equipment, yet it can cause widespread flooding due to ice jam blowouts during the melt season, endangering community residents and infrastructure (Ashton, 1986; Beltaos, 2013; Hicks, 2016; Nakanishi and Dorava, 1994; O'Neill and Arcone, 1991). These consequences vary each year due to changes in local weather and climate (Beltaos, 2013).

In remote rural Alaska, stretching from the North Slope to the Alaska Peninsula, are hundreds of small communities, half of which are not connected by formal transportation routes (i.e., roads and highways) (Belz and Chang, 2018; Goldsmith, 1990). Some of these communities are only accessible by plane or boat during the summer. In winter, during the coldest months of the year, many rural communities rely on frozen rivers, lakes, and other waterways to provide access via ice roads and trails. Ice roads provide a corridor for moving heavy equipment,

* Corresponding author.
E-mail addresses: sveta.stuefer@alaska.edu (S. Stuefer), rrangel2@uwyo.edu (R.C. Rangel), cvmaio@alaska.edu (C. Maio), npbelz@alaska.edu (N. Belz), ronald.daanen@alaska.gov (R. Daanen).

https://doi.org/10.1016/j.coldregions.2023.103819
Received 28 April 2022; Received in revised form 2 December 2022; Accepted 4 March 2023
Available online 8 March 2023

supplies, and fuel, which otherwise are expensive to ship as air cargo (Kiani et al., 2018). River ice cover commonly has recreational use by people on foot, skis, or snowmachine. The use of river ice roads and trails can be dangerous depending on integrity of ice, local hydraulic hazards, and loads placed on the floating ice cover. In addition, accelerated climate warming shortens the length of the ice road season (Osborne et al., 2018; Stephenson, 2012) .

Common hydraulic hazards with river ice roads include overflow, ice thickness variability, and wet and dry cracking, while engineering hazards include snow drifting (Saskatchewan Winter Roads Handbook, 2010). In this paper, *overflow* is defined as unfrozen water superimposed on river ice cover and is further expanded on in the following section. Seasonal climate variability has a strong impact on the timing of freeze-up and break-up; the reduced length and warmer temperatures of the cold season prevent ice cover growth and affect ice composition (Dibike et al., 2011; Kiani et al., 2018; Mullan et al., 2017). Using the Canadian Global Climate Model SRES A2 emissions scenario, Dibike et al. (2011) determined that future lake ice duration in northern Canada will decrease by 15–50 days and that lake ice thickness will decrease by 10–50 cm, with the largest reductions occurring at higher latitudes. Due to the rapidly changing climate in northern high latitudes (Mullan et al., 2017), there is a pressing need to determine an accurate, safe, and cost-effective method of measuring structural ice thickness in order to maintain these critical transportation lifelines in a safe manner.

The focus of this research is field measurements of ice cover thickness on the Tanana River and the Yukon River in Interior Alaska, two rivers that span a large portion of the state and are integral to community life in remote rural areas, providing necessary and recreational transportation routes and access to nearby communities. The objective of this paper is to evaluate the accuracy and limitations of ground penetrating radar (GPR) to measure ice thickness under various environmental conditions. Our analysis is specifically targeted at GPR measurement error that occurs from assuming an average radar velocity through variable ice thickness, snow cover, and overflow, all of which are typical of northern rivers. We also test whether the presence of frazil ice affects accuracy of ice thickness measurement due to interference with GPR signal at the base of the ice cover. Additionally, we attempt the identification of vertical layering of river ice types using the common midpoint (CMP) GPR method.

2. Background

Ground penetrating radar is a noninvasive geophysical method that uses high frequency electromagnetic signal (usually 10 to 1500 MHz) to image the subsurface, based on electromagnetic properties of the medium, particularly the dielectric permittivity (Daniels, 2000; Neal, 2004). The greater the contrast in relative dielectric permittivity, the greater the reflection strength in the resulting radargram (Olhoeft, 1998). The relative dielectric permittivities for river ice, freshwater, and snow are 3–4, 80, and 1.5–2, respectively. Fu et al. (2018) inferred that this variance in dielectric permittivity for river ice and snow is a result of various types of ice formation with different ice densities. Therefore, we assumed that dielectric properties differ between layers of river ice with varying gas content and density.

Ground penetrating radar has been successfully used to measure ice thickness on lake, river, sea, and laboratory-formed ice (Annan et al., 2016; Galley et al., 2009; Proskin et al., 2011; Li et al., 2010). Some studies (Fu et al., 2018; Proskin et al., 2011) used double antenna systems to simultaneously measure floating ice thickness and water depth underneath. On sea ice, GPR could be applied to identify the interface between warm wet saline ice and cold ice (Maijala et al., 1998). Ground penetrating radar was tested to measure spatial variation of river ice thickness on the Pulmanki River in northern Finland, with a mean absolute error of approximately ±3 cm (Kämäri et al., 2017) when comparing GPR measurements to ground truth measurements of ice thickness. Additionally, GPR was used to simultaneously measure the thickness of snow and ice layers with an error of ±2 cm and < 2 cm (also compared with ground truth measurements), respectively (Liu et al., 2013). Some GPR systems such as Sensors & Software IceMap™ are designed specifically for ice thickness measurement with instant readout by assuming a constant velocity of the signal wave as it penetrates the ice cover. These readings have an approximate error in radar velocity ranging from ±2% to ±7%, with smaller errors occurring at thicker ice and larger errors occurring at thinner ice (Annan et al., 2016).

Literature review shows that electromagnetic wave velocity in freshwater ice can vary substantially, from 0.130 to 0.206 m/ns depending on ice type, thickness, and age (Finlay et al., 2008). Turbulent river ice formation is different from that of calm lake ice formation due to constant water flow that results in heterogeneous spatial distribution of ice types in rivers. This difference results in pancake ice, floes, frazil ice, and slush on rivers, while on still, frozen lakes only two layers are common: snow ice and lake ice (Gow, 1986; Michel and Ramseier, 1971). River ice can be discussed in terms of three ice cover types—primary, secondary, and superimposed ice—all of which differ under diverse and variable river and climate conditions (Ashton, 1986; Michel and Ramseier, 1971). In this paper, primary ice cover refers to frazil ice, the first formed ice in turbulent water. Secondary ice refers to columnar ice, which forms as a result of heat fluxes at the ice cover surface (Dibike et al., 2011). Superimposed ice refers to snow ice, which forms due to overflow freezing together with snow cover. These varying river ice types can generally be identified by collecting ice cores.

Overflow can occur as a result of sagging ice cover due to the weight of snow cover, vehicles, and equipment placed on ice. This added weight can cause depression in the ice cover surface beneath the water surface elevation, which allows for water to flow onto the ice cover through cracks or open leads (Beltaos, 2013). Overflow can be unpredictable in relation to snow depth on ice cover due to variances in source, but frequently occurs near riverbanks and at hinge cracks on river edges due to stage change or increased snow load (Ashton, 2011). In permafrost regions, river and stream overflow can also occur when a change in hydrostatic pressure pushes groundwater onto the ice surface (Schneider et al., 2013; Ensome et al., 2020); however, this subject goes beyond the scope of our study.

In river ice research, Osterkamp and Gosink (1983) documented a large production and accumulation of frazil ice on the Tanana River. This type of ice forms in turbulent sections of a river when water particles are supercooled in an open lead and flocculate as they flow downstream (Beltaos, 2013; Daly, 2013; Hicks, 2016). Frazil ice can collect in such large quantities that the conveying capacity of ice-covered rivers is significantly affected by the reduced cross-sectional area (Marko and Jasek, 2008). Additionally, when frazil ice becomes frozen to the bottom of floating ice cover, it increases the ice cover thickness. Several studies discussed detection and characterization of frazil ice using GPR. Annan and Davis (1977) hypothesized that an extra reflection in their radargrams below the ice cover was frazil ice accumulation. Arcone et al. (1987) tested GPR and magnetic induction conductivity method for detecting frazil ice on the Tanana River.

Though river ice roads and trails are typically built on or naturally follow the thickest ice locations, river ice still has a highly variable nature. Therefore, monitoring methods that accurately provide detailed measurements of ice thickness and ice type under different conditions on rivers are necessary. Natural phenomena such as snow, snow ice, and air bubbles in river ice cover affect the bulk radar velocity measured with GPR. As air content increases, the radar two-way travel time (TWT) decreases, which can result in an underestimation of ice thickness (Zhi-Jun et al., 2010).

3. Study area

River ice data collection occurred at two locations in Interior Alaska (Fig. 1a). These locations are the Yukon River near the city of Tanana (Fig. 1b), and the Tanana River near the city of Fairbanks (Fig. 1c).

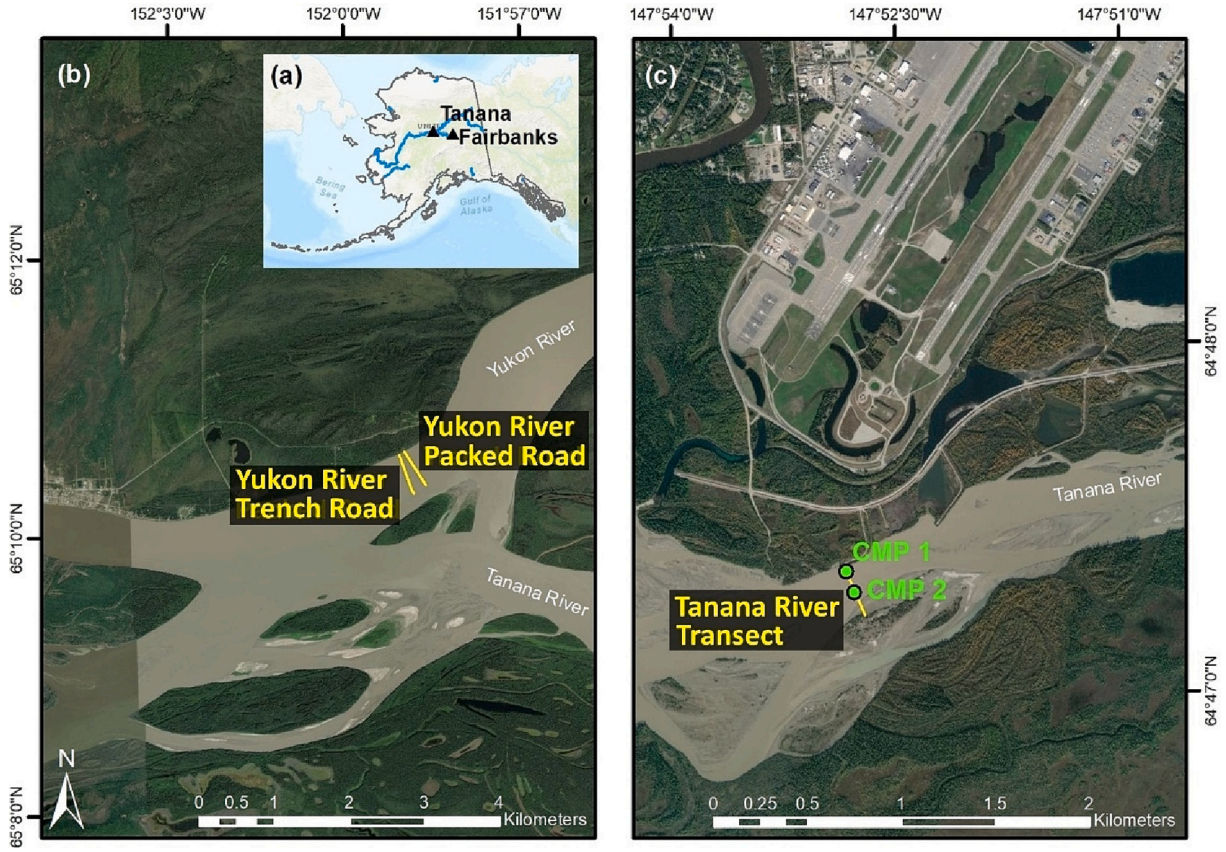

Fig. 1. (a) Map of Alaska. (b,c) Detailed maps of river ice data collection locations on the Yukon River ice roads east of Tanana (b) and on the Tanana River southwest of Fairbanks city center (c), including locations of common midpoint (CMP) method, Tanana River transect.

Tanana is located approximately 210 km (130 miles) northwest of Fairbanks. Both locations are subject to long cold seasons from October to March, when mean monthly air temperatures stay below freezing.

The Tanana River study site near Fairbanks is collocated with a United States Geological Survey (USGS) gauging site (ID 15485500). The USGS Fairbanks field office conducts repeated stream flow measurements across the Tanana River main channel (Fig. 1c). This transect where we collected river ice measurements is near a trail on the river ice cover commonly used by people on skis and snowmachines. The transect extends from the north bank (64.7910, −147.8837) to the south bank (64.7896, −147.8819). The average temperature in Fairbanks for the 2018/2019 cold season was −11.0 °C (12.2 °F); for the 2019/2020 cold season it was −15.8 °C (3.5 °F). The climate normal mean cold season temperature from 1991 to 2020 was −15.1 °C (4.8 °F); mean annual air temperature (1991–2020) was −2.1 °C (28.3 °F).

We performed GPR data collection at the Tanana River location in March 2019 and February 2020. The Tanana River ice cover at this location includes primary, secondary, and superimposed ice types, making it an ideal example of river ice formation in Interior Alaska. A distinctive feature at this location is frazil ice that accumulates beneath the ice cover, blocking flow over a large portion (up to approximately 50%) of the cross-sectional river area.

The Yukon River study site was located approximately 2 miles (3.2 km) upstream of Tanana and consisted of two ice roads. This transportation route is maintained by Tanana to connect the community to the state road system that ends 6 miles (9.7 km) upstream on the south side of the Yukon River (see Fig. 1b).

We performed data collection at the Yukon River study site in February 2020. During that winter (2019/2020), unlike winters before, Tanana had established two ice roads to help in determining the best ice road building method for future years (Stuefer and Richards, 2021). These two roads are referred to as the “Trench Road” and “Packed Road” (Fig. 2), and their location was chosen because high-speed winds there remove snow cover, which allows river ice to grow faster. Another characteristic of this location is rough (juxtaposed) ice cover, which occurs due to ice jamming during freeze up.

Trench Road was formed by consistently clearing snow off the ice and leveling the road so that cold could better penetrate existing ice to thicken the ice cover. Packed Road was built by breaking down the rough ice at the surface of the ice cover and packing it down by dragging a groomer over the snow and ice. The goal at Packed Road was to minimize snow berms that cause large snowdrifts. Extensive overflow occurred at the beginning of the 2019/2020 winter, potentially due to the heavy snow load that resulted from snowfall early in the season. This study location typically does not have frazil ice accumulation and is therefore a good site to compare with the Tanana River location. All transects at both locations are summarized in Table 1.

4. Methods and data

We performed GPR surveys along with manual ice thickness measurements on each river transect. Two GPR methods were used to determine radar velocity: common offset and common midpoint (CMP). The resultant data were processed using standard routines. Field data collections are summarized for the years 2019/2020: one winter season on the Yukon River and two winter seasons on the Tanana River. For simplicity, the trail on the Tanana River and the two roads on the Yukon River are all referred to as ice roads.

4.1. Manual measurements of ice thickness and snow depth

We collected ice thickness measurements by drilling holes in the

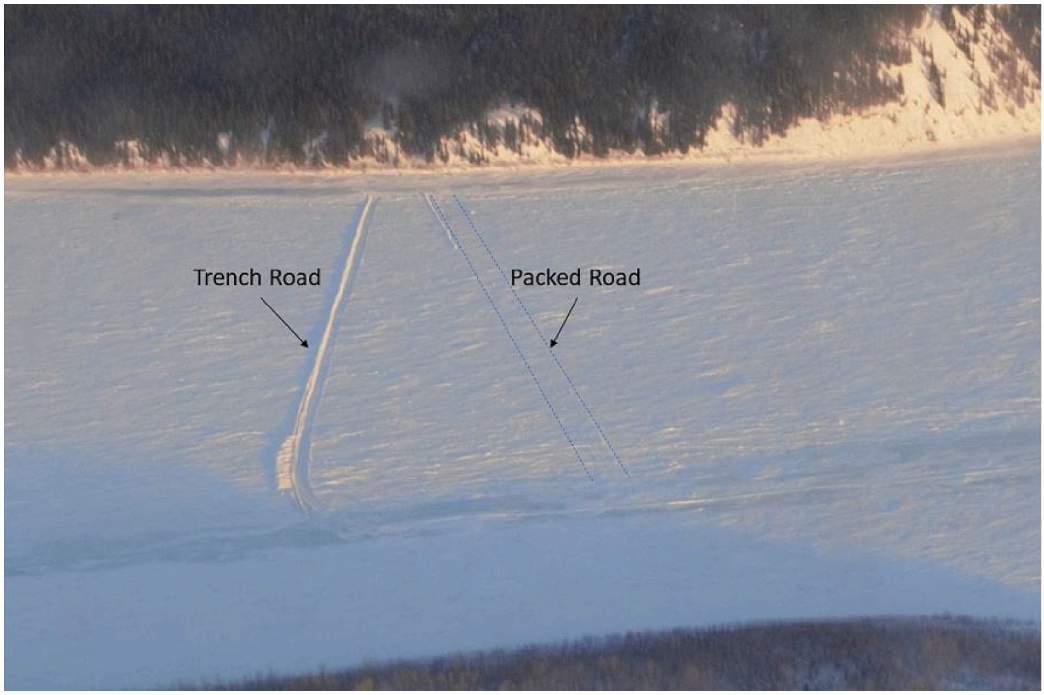

Fig. 2. Trench Road (left) and Packed Road (right, marked by dashed lines) on the Yukon River.

Table 1
Summary of GPR profiles collected at Tanana River (TR) and Yukon River (YR) and number of manual ice thickness measurements taken during surveys (N).

Profile ID	Date	City	River	Length (M)	Tair (^{0}c)	Frequency (MHZ)	N
TR19_450SN	23Mar2019	Fairbanks	Tanana	164.5	4	450	22
TR20_450NS	03Feb2020	Fairbanks	Tanana	107.8	−14	450	23
TR20_800CMP	06Mar2020	Fairbanks	Tanana	1.0	−30	800	2
YR20T_450NS	27Feb2020	Tanana	Yukon	460.7	−28	450	13
YR20T_750NS	27Feb2020	Tanana	Yukon	520.2	−28	750	13
YR20P_450NS	27Feb2020	Tanana	Yukon	493.9	−28	450	3
YR20P_750NS	27Feb2020	Tanana	Yukon	526.7	−28	750	3

river ice along the GPR survey line. We used a measurement rod with a toe at the bottom to measure ice thickness by matching the toe of the rod to the bottom of the ice cover, and determined the depth of frazil ice by pushing the rod through the frazil until it reached open water. Overall, we collected 79 manual ice thickness measurements ($n = 79$) over approximately 2300 m distance (Table 1). We used a snow depth rod to collect 3 manual measurements of snow depth around each ice hole and measured bulk snow density with a snow corer at 3 locations across the river (Stuefer et al., 2020).

4.2. GPR data collection

For common-offset measurements, we used a MALÅ (Guideline Geo, Sundbyberg, Sweden) GroundExplorer (GX) GPR instrument with 450 MHz and 750 MHz central frequency antennas to image river ice and estimate ice thickness at both study locations (Table 1). This instrument consists of a unit containing the transmitter and receiver antennas (18 cm and 14 cm offset for the 450 MHz and 750 MHz antennas, respectively) and a separate control unit monitor. The system has a built-in differential global positioning system (GPS) and records simultaneous location and radar pulse data at a fixed distance (if using an encoding wheel) or time increment. The transmitter/receiver unit was towed along the ground surface by foot to collect a transect perpendicular to the river shoreline. At each location, we collected a transect in both the north and south directions. Digital surface markers were placed during the transect collection to mark ice measurement locations for easier comparison and analysis after the survey. We chose the radargram with the most completeness and highest qualitative signal-to-noise ratio for each transect location in instances where repeat profiles were collected, resulting in a final total of 7 transects. Completeness was defined as the number of points with a definite ice-water interface reflection. Additionally, we used a MALÅ ProfessionalExplorer (ProEx) with two 800 MHz central frequency antennas to perform two CMP measurements at the Tanana River study location.

The ice thickness data discussed in the Results section were collected from only the south directional transects due to the higher quality of these radargrams. An example of a radargram from the Yukon River is shown in Fig. 3a; a simple visual analysis of common reflections in the collected GPR data is shown in Fig. 3b.

4.3. Ice radar velocity and thickness estimation

We estimated the ice radar velocity and relative permittivity based on the GPR two-way-travel time (TWT) for the ice layer and the collocated manual ice thickness measurement using the following equation (Neal, 2004):

$$v = \frac{d_m}{TWT/2} = \frac{c}{\sqrt{\epsilon_r}} \quad (1)$$

Where ν is the wave velocity (m/ns), d_m is the manual ice thickness measurement (m), c is the speed of light (0.2998 m/ns), and ϵ_r is the

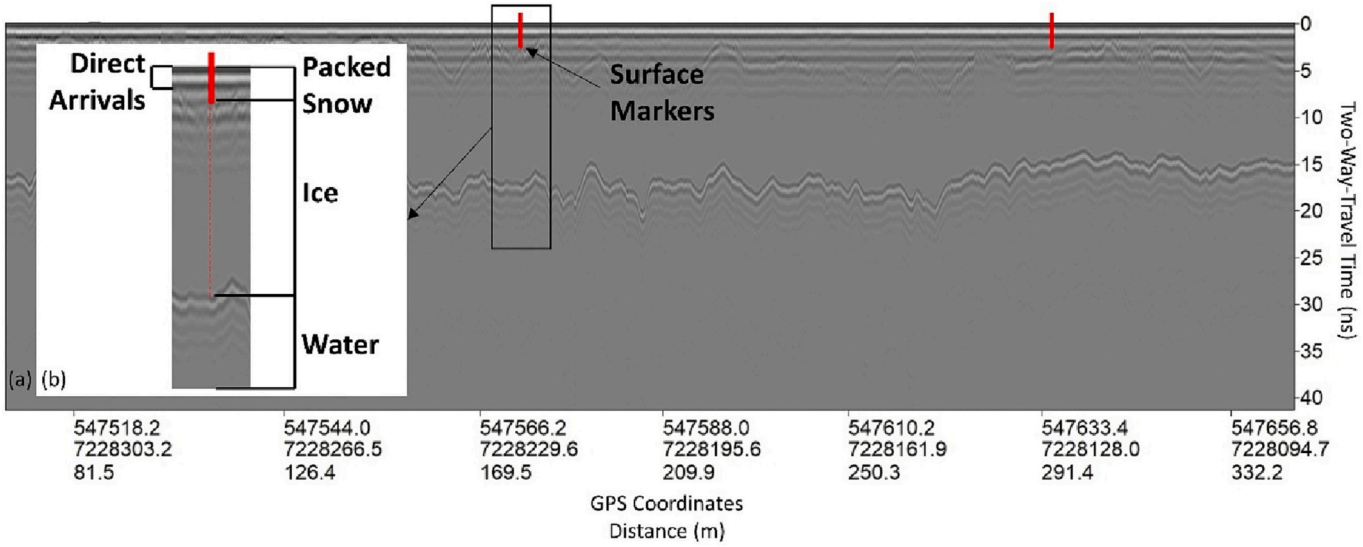

Fig. 3. (a) A section of the radargram from the Yukon River Packed Road at 750 MHz. This radargram can be analyzed for various layers: (b) packed snow and ice cover layers; airwave arrivals refer to the portion of the radar wave that travels directly from the transmitter to the receiver. Surface markers, indicated by short red lines, were placed during the transect at each location where hand measurement of ice thickness was collected. (For interpretation of the references to colour in this figure legend, the reader is referred to the web version of this article.)

relative permittivity of the material the wave is traveling through. Next, based on the average ice radar velocity, we estimated the ice thickness for the whole GPR transect with the following equation:

$$d_c = \frac{v^{*}TWT}{2} \quad (2)$$

where d_c is the calculated ice thickness (m), and *TWT* is the time it took for the wave signal to reflect to the receiver (ns). The calculated ice thickness is affected by the distance between the GPR transmitter and receiver antennae, commonly referred to as *offset*. The zero-offset approach is assumed because the antennae offset (14 and 18 cm in our case) is considerably smaller than the measured ice thickness. These are the basic equations used to determine ice thickness in GPR instruments such as IceMap™, mentioned previously.

4.4. Common offset GPR data processing

We used 3 software packages to process the GPR data: RadExplorer, ReflexW, and GPR-SLICE. Created for use with MALÅ systems by Guideline Geo, RadExplorer is used for 2D data and includes several processing routines standard to most GPR softwares. We extracted ice thickness estimation for initial analysis by hand selecting the first break for each major reflection in RadExplorer. GPR-SLICE and ReflexW are independent GPR data synthesis programs capable of analyzing 2D data. They were used to produce individual trace plots and figures for this paper.

We applied minimal processing routines to preserve signals for the ice radar velocity estimation. In the order listed, we used the following RadExplorer processing routines on the data after collection: Time Zero correction (used to move the start time to first airwave arrival), DC Removal (used with default values on mean mode to remove constant component of signal), Trace Edit (vertical crop used to remove the unnecessary vertical portion of the radargram), Spatial Interpolation (used with default dL to attempt to smooth data), and Bandpass Filtering with default values provided by RadExplorer to filter out excess noise. Additionally, a small constant gain was applied for clarity of the reflections. Due to the ice surface being effectively flat, there was no need to correct for surface elevation at these locations.

4.5. Defining snow-ice and ice-water interfaces

An airwave signal, present at the top of each radargram, masks the snow-ice interface reflection in most cases (this signal varies in time depending on the snow depth and the central frequency of the GPR antennas). The only transect in which the snow-ice interface is visible is at Packed Road on the Yukon River, for which the accuracy analysis was not completed due to limited ground truth measurements. An additional processing routine, Background Removal, is available to remove the airwave signal that masks the interface between snow and the top of the ice cover. However, this processing routine did not produce a clear snow-ice interface reflection and therefore was not used on this dataset.

In order to calibrate the snow-ice interface, we used snow data, radar velocity, and two-way travel time (Eq.1). We converted the hand-measured snow depth to TWT based on an assumed velocity of 0.212 m/ns through dense snow (Brandt et al., 2007), which is subtracted from the total TWT between the first breaks of the airwave arrival and the ice-water interface reflection. Fig. 4 depicts a sample of the airwave arrival and the snow-ice and ice-water interface reflections. The velocity through snow is assumed based on density measurements and general knowledge of snow cover at the study locations. The resulting value is the estimated TWT only through the ice cover.

Manual ice thickness measurements were divided in calibration/validation datasets to ensure a representative range in thickness and to provide enough points for validation analysis. For calibration dataset, the average radar ice velocity was determined (using Eq. 1) from 1/3 of the manual snow depth and ice thickness measurement locations (chosen as every third point) on each transect where TWT for the ice-water interface could be determined from the radargram. This average velocity model was used to calculate ice thickness at the remaining 2/3 of data points (validation dataset), which were compared with the hand-measured ice thickness (ground truths). Root mean square error (RMSE) and mean absolute error (MAE) were calculated to analyze the accuracy of using an average velocity model by comparing the ice thickness based on the GPR and the manual measurements.

4.6. Common midpoint method

We applied the common midpoint (CMP) method to attempt the identification of possible layers of varying ice types (and therefore

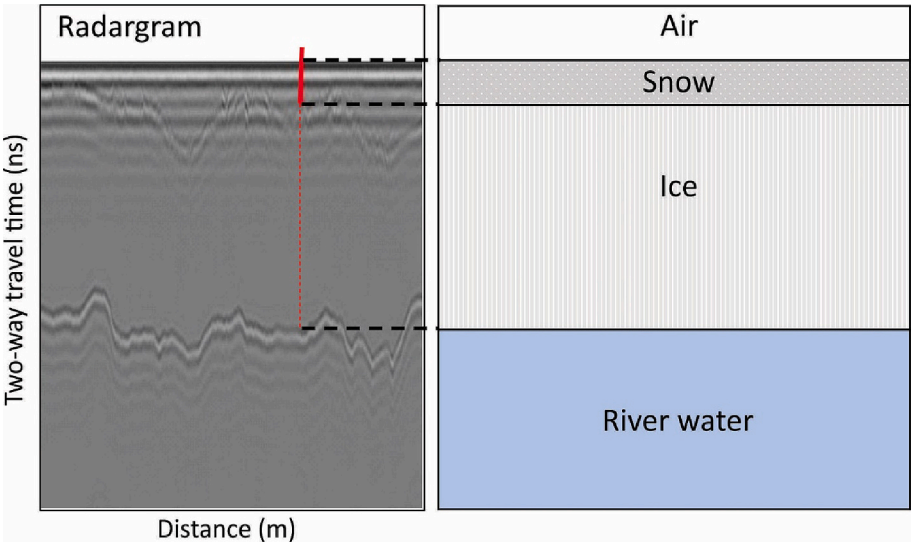

Fig. 4. A borehole is shown on a sample GPR radargram at the location of a surface marker (short red line). The borehole is traced by a dashed red line that indicates the ice layer. The TWT for hand-measured snow depth around this borehole is subtracted from the TWT between the airwave arrival and the ice-water interface reflection to leave only the TWT for the ice layer for the ice velocity estimation.

varying dielectric permittivities) in river ice cover. We performed a CMP analysis on the Tanana River at the same location as the common offset transects to parse these ice layers. For this analysis, the CMP length was 1 m, with a trace spacing of 0.10 m, and the first offset of 0.2 m. Two shielded bistatic antennas (each with a frequency of 800 MHz) were placed at a set distance and moved apart at the fixed small interval of 0.10 m. Before the CMP measurement, we performed an air shot measurement where the antennas were held in the air and pointed to each other, and a radar velocity for the air was estimated (i.e., the speed of light ~0.3 m/ns). We used ReflexW to fit velocity curves to the CMP dataset, and thereby estimate the radar-wave velocity (normal moveout velocity) for the river ice layer. This method of GPR has been successfully used to simultaneously measure snow and sea ice thickness with MAE of 2 cm (12%) and <2 cm (4%), respectively (Liu et al., 2013). Parsekian (2018) successfully used the CMP method to identify reflections at interfaces of ground-fast ice and subsurface layers of sand, gravel, and saturated gravel aquifer, as well as water content in these layers. Therefore, we expected that CMP analysis could identify variance in layers of river ice types if there was enough contrast in electrical permittivities.

We performed CMP data collection on the Tanana River transect on March 6, 2020 (Table 1). We removed snow at the CMP survey locations and performed two CMP collections, but only collected a manual ice thickness measurement at CMP1 to estimate the bulk ice radar velocity. The location of CMP1 was close to the north bank, near the river thalweg; the location of CMP2 was near the middle of the transect (Fig. 1c).

5. Results

We have summarized the GPR river ice measurements in terms of three ice conditions that commonly occur on rivers used for winter travel in rural Alaska: 1) river ice with snow cover and overflow, 2) river ice with snow cover, and 3) bare ice (Fig. 5).

5.1. Condition 1: River ice with snow cover and overflow

The river ice with snow cover and overflow present was observed on the Tanana River in March 2019 (Table 1, TR19_450NS; Fig. 6). Overflow occurred due to water rising through auger holes drilled the day before. River water accumulated on top of the ice cover and saturated bottom layers of the snowpack. Overflow was not readily visible from

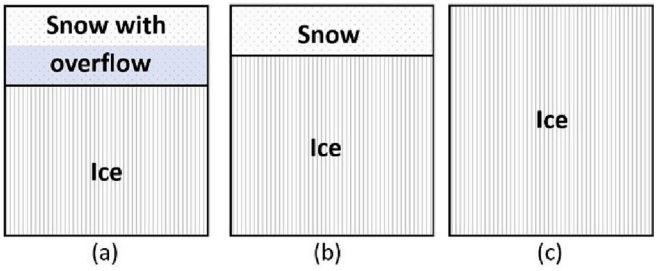

Fig. 5. An illustration of the three ice conditions analyzed in this study: (a) Condition 1, river ice with snow cover and overflow; (b) Condition 2, river ice with snow cover, and (c) Condition 3, bare ice.

the riverbank. The depth of overflow varied from 11 to 18 cm, measured at points 7 through 18, marked with blue squares in Fig. 6a. The snow cover had an average depth of 0.32 m, ranging from 0.16 to 0.43 m (the smaller values tend to be due to trampled snow around the ice measurement hole). Snow was dry and light, except for the overflow section with standing water at the bottom of the snowpack. The river ice varied in thickness from 0.5 to 1.2 m based on 22 hand measurements (Fig. 6a). Loose crystals of frazil ice were observed under the ice cover at several locations, completely filling the cross-sectional area close to the left bank (cross-hatched area in Fig. 6a). Frazil ice accumulation varied in thickness from 0.38 to 0.70 m. Overflow, snow depth, ice thickness, frazil ice deposition, and water depth outlining channel profile (Fig. 6a) are all measured in the field manually.

GPR measured ice thickness could only be deduced from the radargram at 11 out of 22 points; we could not retrieve ice thickness at the remaining half of the data points due to the presence of overflow at those locations. The average calculated radar wave velocity through the river ice was 0.156 m/ns; this calculation was based on 1/3 of the manually measured ice thickness data points (shown as squares in Fig. 6c). The top and the bottom of the river ice cover are marked with light blue and dark blue horizons, respectively (Fig. 6b). Average velocity was used to create a model (black line in Fig. 6c), using Eq. 2 to calculate river ice thickness from TWT measured by GPR. The accuracy of this model was evaluated with the remaining 2/3 of the data points (shown as circles in Fig. 6c). The GPR-calculated ice thickness varied from 0.78 to 1.18 m. No additional reflections were observed beneath the ice-water interface to

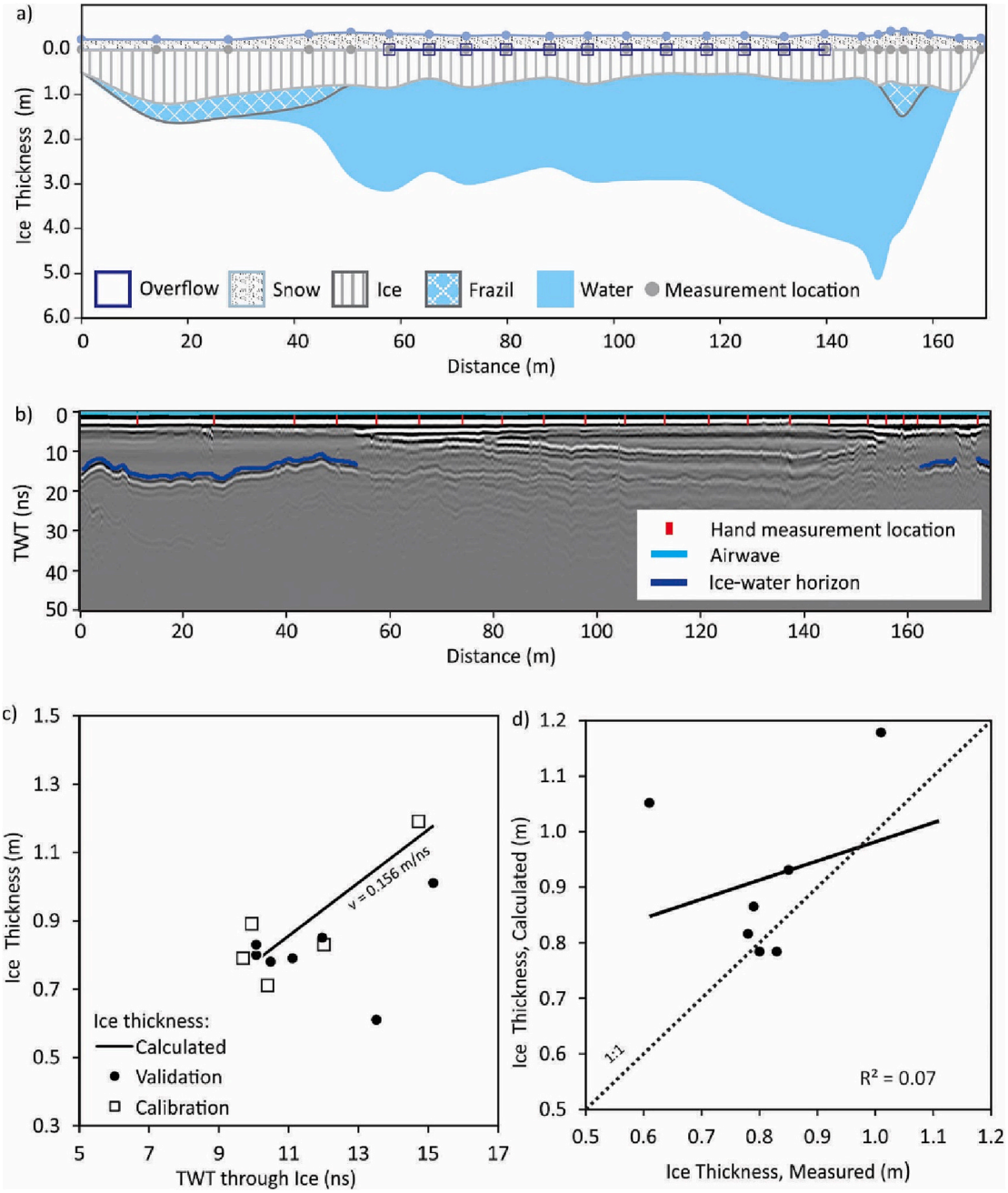

Fig. 6. Data collection and analysis summarized for Condition 1 from the Tanana River in 2019. (a) Hand measurements of river ice thickness, snow depth, frazil ice, and water depth; blue squares mark the points with overflow present. (b) Radargram data collected on the transect; horizons added as a visual aid below; red dashes show locations of manual snow and ice measurements. (c) Average velocity model with calculated thickness as a line and hand-measured ice thickness plotted against the TWT through ice. Squares represent hand-measured ice thickness used to calculate average velocity (calibration), while circles show remaining hand-measured ice thickness used for validation. (d) Regression plot for TR19_450SN of measured ice thickness against average velocity model ice thickness compared to a 1:1 relationship. (For interpretation of the references to colour in this figure legend, the reader is referred to the web version of this article.)

indicate changes in relative dielectric permittivity due to the presence of frazil ice.

For these ice conditions, the level of error between measured and calculated ice thickness was relatively high. The RMSE for the manually measured ice thickness compared with the calculated ice thickness was 0.185 m, and the MAE was 0.124 m (Fig. 6c). The R^2 value for this condition was as low as 0.07 (Fig. 6d).

5.2. Condition 2: River ice with snow cover

The second condition analyzed was river ice with snow cover present (Fig. 7). This condition was observed on the Tanana River in 2020, as well as on the Yukon River Packed Road in 2020 (Table 1; rows 2, 6, 7). An average of 0.27 m of snow ranging from 0.06 to 0.37 m (Fig. 7a) covered the Tanana River. The measured ice thickness varied from 0.44 to 0.91 m (n = 23). Frazil ice also accumulated at this section of the Tanana River in 2020, and varied in thickness from 0.70 to 1.91 m. Snow depth, ice thickness, frazil ice accumulation, and water depth outlining channel profile (Fig. 7a) are measured in the field manually.

The average calculated radar wave velocity through the river ice was 0.156 m/ns, using Eq. 2, TWT, and 1/3 of the manually measured ice thickness points (shown as squares in Fig. 7c) . GPR ice thickness could

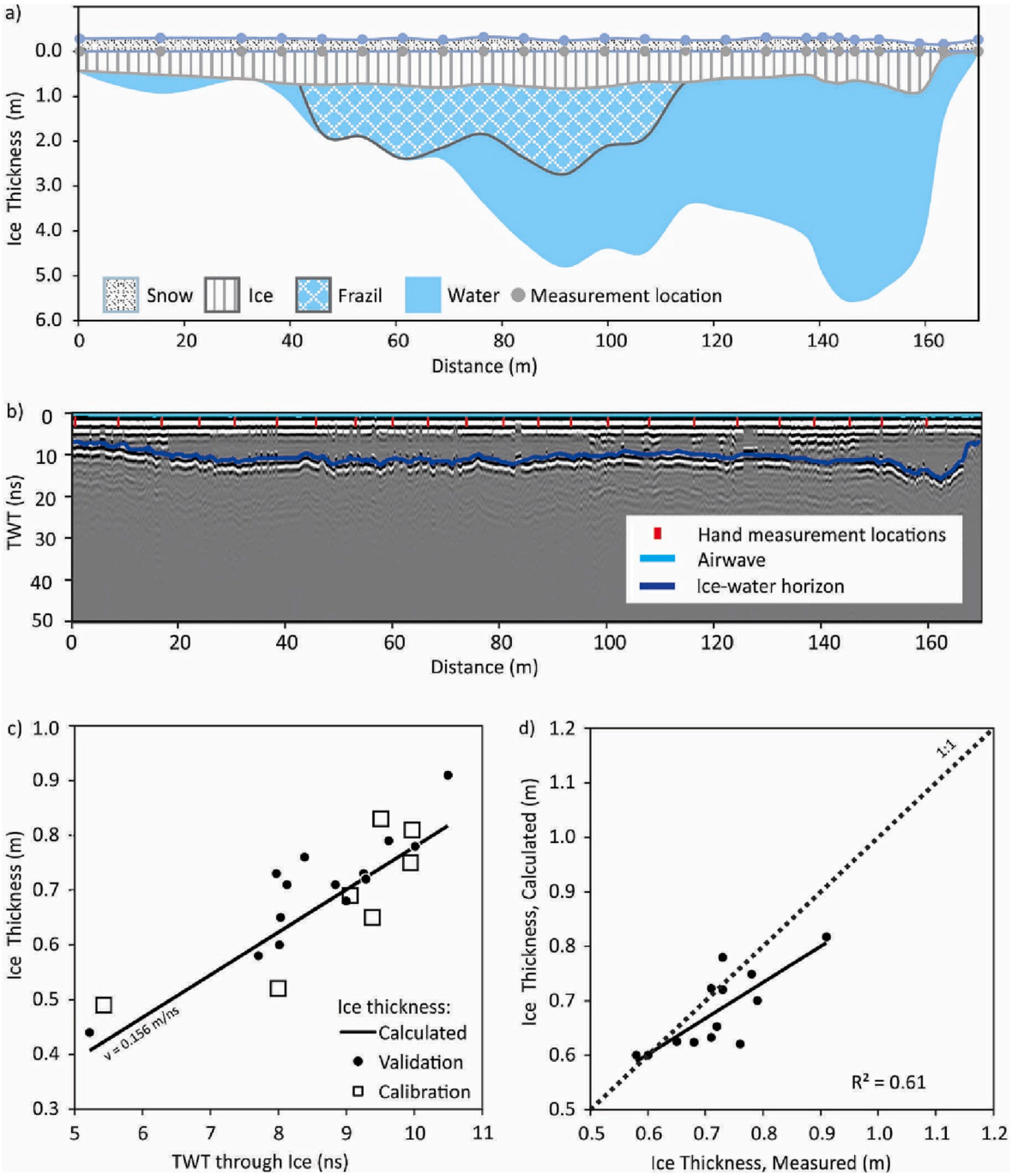

Fig. 7. Data collection and analysis is summarized for Condition 2 from the Tanana River in 2020. (a) Hand measurements of river ice thickness, snow depth, frazil ice, and water depth. (b) Radargram data collected on the transect; horizons added as a visual aid below; red dashes show locations of manual snow and ice measurements. (c) Average velocity model with calculated ice thickness as a line and hand-measured ice thickness plotted against the TWT through ice. Squares represent hand-measured ice thickness used to calculate average velocity (calibration), while circles show remaining hand-measured ice thickness used for validation. (d) Regression plot for TR20_450NS of measured ice thickness against average velocity model ice thickness compared to a 1:1 relationship. (For interpretation of the references to colour in this figure legend, the reader is referred to the web version of this article.)

be deduced from the radargram at a total of 21 out of 23 hand-measured points. The average velocity model ice thickness (black line in Fig. 7c) is evaluated against remaining 2/3 of auger points (shown as circles in Fig. 7c). The calculated ice thickness varied from 0.41 to 0.82 m. For this condition, RMSE and MAE were much smaller, 0.06 m and 0.042 m, respectively (Fig. 7c). The R^2 value of 0.61 indicated a closer agreement between hand-measured and radar-calculated ice thickness (Fig. 7d).

The trace plots for unedited radargrams were analyzed qualitatively to detect reflection from frazil ice crystals that were regularly present in the river water at the Tanana River transect. Visual inspection was used for comparison of the trace plot from locations on the transect without frazil ice (Fig. 8a) with a trace plot from a location with frazil ice (Fig. 8b). Based on the interpretation methods, the dielectric contrast was too weak to produce a distinguishable difference in the returned signal from the ice-water interface versus the ice-frazil interface with the radar frequencies used.

On the Yukon River, we observed dense wind- and groomer-packed snow with an average of 0.15 m depth. There was no frazil ice

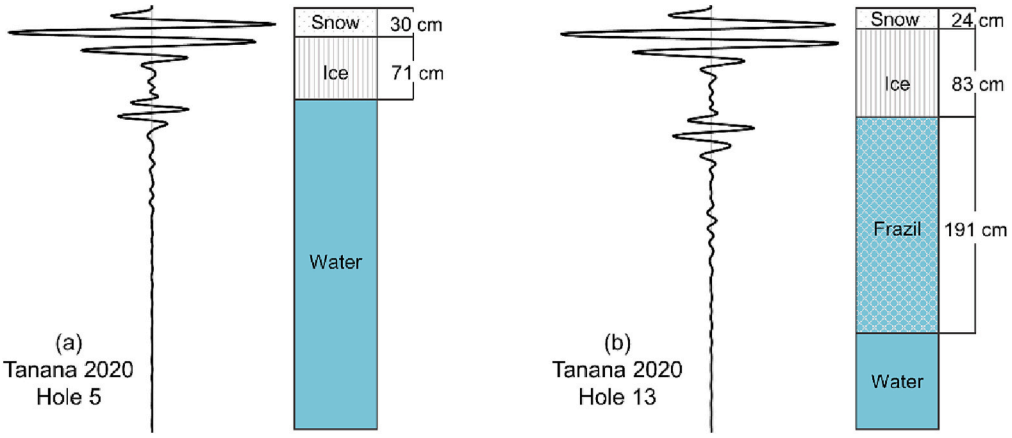

Fig. 8. Trace plots from the 450 MHz antenna for two different conditions: (a) snow only on ice cover and (b) the addition of frazil ice in water. Trace plots shown side-by-side to determine the effect of frazil on radar reflection.

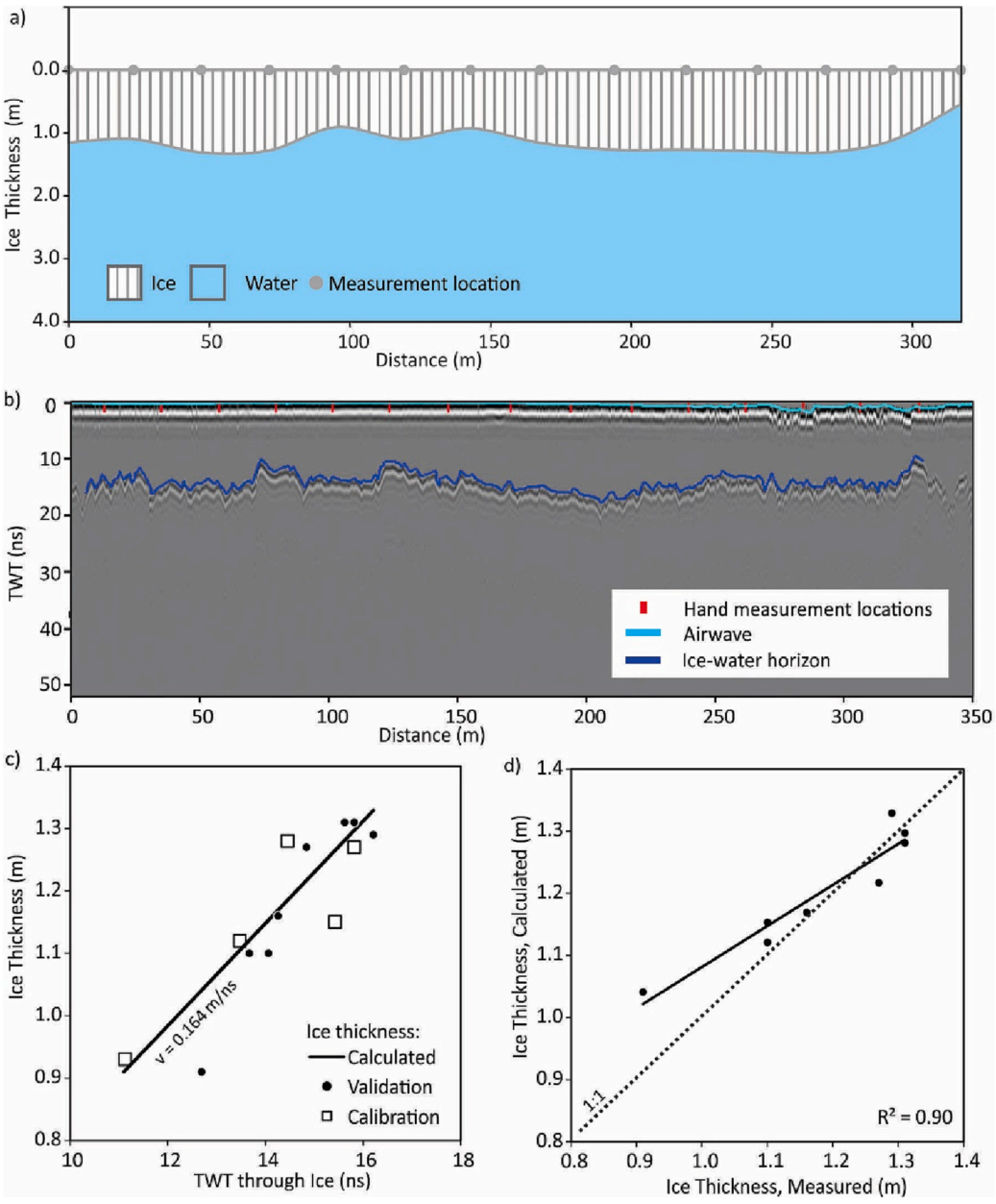

Fig. 9. Summary of data collection and analysis for the Yukon River Trench Road. (a) Hand measurements of river ice thickness and snow depth. (b) Radargram data collected on the transect, horizons added as a visual aid below; red dashes mark 17 locations of manual snow and ice measurements on the GPR transect, though ice thickness could only be manually measured from 13 holes. (c) Average velocity model with calculated ice thickness as a line and hand-measured ice thickness plotted against the TWT through ice. Squares represent hand-measured ice thickness used to calculate average velocity (calibration), while circles show remaining hand-measured ice thickness used for validation. (d) Regression plot for YR20T_450NS of measured ice thickness against average velocity model ice thickness compared to a 1:1 relationship. (For interpretation of the references to colour in this figure legend, the reader is referred to the web version of this article.)

accumulation on this section of the river. Only 3 hand measurements of ice thickness were collected on the Packed Road. For these points, the average calculated radar wave velocity through the river ice was 0.170 m/ns for both the 450 MHz and the 750 MHz antenna, while the calculated ice thickness varied between 1.21 and 1.42 m for the 750 MHz antenna and 1.28–1.45 m for the 450 MHz antenna. The Yukon River Packed Road radargram is shown earlier in the text (see Fig. 3). An accuracy analysis was not completed for this location due to the limited number of ice thickness measurements.

5.3. Condition 3: Bare ice

The last condition analyzed was bare ice—no snowpack or overflow present. This condition was observed on the Yukon River Trench Road and a portion of the Tanana River where snow was manually removed. No snow was present on the Trench Road due to consistent clearing by the town. The ice varied in thickness from 0.91 to 1.31 m ($n = 13$) under this road (Fig. 9a). Frazil ice was not observed at this Yukon River location.

Manual ice thickness measurements were attempted at 17 locations (marked on the radargram in Fig. 9b); however, measurements were only collected at the first 13 holes (the first 13 red dashes in Fig. 9b). Ice thickness calculated by GPR could be deduced from the radargram at all 13 locations of manual measurements. Calculated ice thickness varied from 1.03 to 1.30 m for the 750 MHz antenna and 1.04–1.33 m for the 450 MHz antenna. The average calculated radar wave velocity through the river ice was 0.164 m/ns for both antennas (model accuracy is summarized in Fig. 9c).

For this condition, the highest level of accuracy was between measured ice thickness and calculated ice thickness. The RMSE for the manually measured ice thickness compared with the calculated ice thickness was 0.06 m; the MAE was 0.044 m (Fig. 9c) for the 750 MHz antenna. The RMSE was 0.05 m and the MAE was 0.036 m for the 450 MHz antenna. The R^2 value for this condition was 0.90 (shown in Fig. 9d).

The CMP analysis on the Tanana River in 2020 fits under Condition 3, as snow (0.15 m depth) was cleared away from the ice cover. Ice thickness measured by hand was 0.76 m. The hand measurement produced a radar velocity of 0.177 m/ns, which matches the velocity curves for CMP1 and CMP2 shown in ReflexW (Fig. 10), though a range of velocities from 0.15 to 0.18 m/ns are a possible fit.

These values are reasonable considering that the general range of velocity in impure ice can vary between 0.150 and 0.173 m/ns (Brandt et al., 2007). The radar velocity of 0.177 m/ns is higher than the average velocity of 0.156 m/ns calculated 1 month earlier (Table 2). The difference in velocities could be attributed to uncertainty caused by uneven ice cover, ice growth during the month, or the presence of more impurities (i.e., encapsulated air) in the section of ice measured for the CMP analysis compared with the entire length of the transect used in the primary analysis. Despite the appearance of lateral variance in river ice-cover properties based on varying average velocities, the CMP analysis did not successfully identify different vertical river ice layers.

5.4. Comparison of varying ice conditions

Compared with other transects, Condition 3 (Yukon River Trench Road) had low error and the highest R^2 value (Table 2). This was so for the Packed Road also, though the limited number of data points decreases the reliability of those statistics.

Note in Table 2 that calculated ice thickness better matches measured ice thickness on the Tanana River in 2020 than in 2019. This difference is most likely due to the presence of overflow and error from uneven snow cover preventing steady movement of the GPR instrument. Additionally, the higher radar velocity calculated from a short section of the Tanana River transect suggests variance in ice cover properties across the river.

6. Discussion

The use of GPR has shown significant promise for understanding and maintaining acceptable levels of safety for residents of remote northern communities traveling on established ice roads. The following discussion addresses the question of whether different conditions of river ice cover affect the usability of a GPR system to analyze river ice cover. We discuss the strengths and limitations of GPR as well, because both are important to understanding this unique way of measuring river ice cover for transportation safety and other engineering applications.

6.1. Increasing the safety of winter travel with GPR measurements

One major strength of GPR is its ability to provide a more extensive understanding of river ice cover than manual measurements alone can provide. While manual measurements are limited to points, GPR collects a complete and continuous radargram of ice thickness at a river cross section. GPR ice measurements are accurate, as proved by the low MAE of 3.6–5.8 cm on an ice cover of 0.91–1.57 m when comparing the average velocity model with ground truth measurements on the Yukon River (Condition 3). This amounts to an error of 2.3–6.4%, therefore,

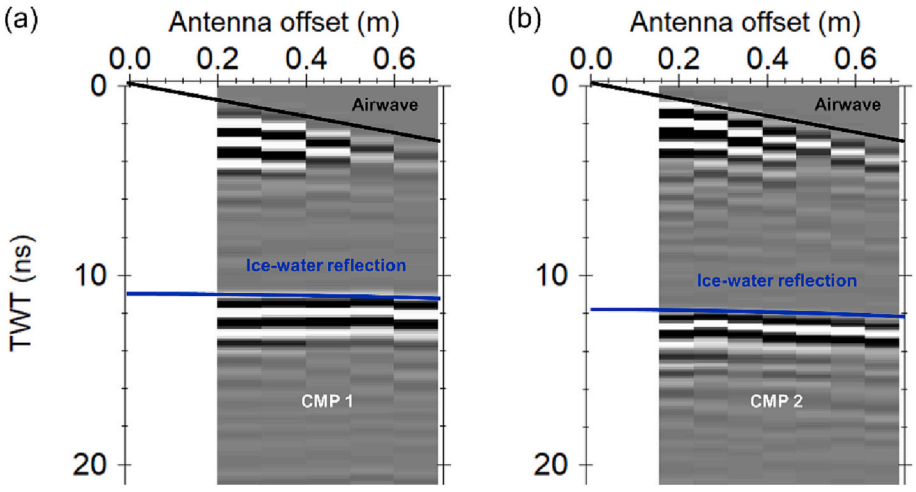

Fig. 10. CMP analysis including the fitting curves to the airwave (0.2998 m/ns) and ice-water reflection (0.177 m/ns). CMP1 (left) was acquired close to the north bank, and CMP2 (right) near the middle of the river (see Fig. 1c).

Table 2
Summary of hand-measured and calculated ice thickness, snow depth, average velocity, MAE, RMSE, and R^2 for all transects.

Location	Year	Antenna (MHz)	Measured Ice Thickness (m)	Calculated Ice Thickness (m)	Average Snow Depth (m)	Average Velocity (m/ns)	RMSE (m)	MAE (cm)	R^2
Tanana River	2019	450	0.50–1.20	0.78–1.18	0.32	0.156	0.164	10.6	0.073
Tanana River	2020	450	0.44–0.91	0.41–0.82	0.27	0.156	0.056	4.2	0.606
Tanana River	2020	800 CMP	0.76	–	0	0.177	–	–	–
Yukon River Trench	2020	750	0.91–1.31	1.03–1.30	0	0.164	0.052	3.6	0.924
Yukon River Trench	2020	450	0.91–1.31	1.04–1.33	0	0.164	0.057	4.4	0.903
Yukon River Packed	2020	750	1.25–1.57	1.21–1.42	0.15	0.170	0.059	5.8	*
Yukon River Packed	2020	450	1.25–1.57	1.28–1.45	0.15	0.170	0.038	3.7	*

*R^2 was not calculated for the Yukon River Packed Road because the dataset only contained 3 hand measurements.

assuming zero-offset and a constant radar velocity through the ice cover is accurate in this case. Having a more comprehensive profile of river ice thickness also allows users to identify areas of thin ice that may not otherwise be detected when collecting manual ice thickness measurements. The GPR unit lends itself well to understanding and maintaining acceptable levels of safety on established ice roads.

6.2. Effect of snow and ice conditions on GPR accuracy

The MALÅ GPR unit produced accurate results for most completed transects. However, it is clear from a visual inspection of the Condition 1 radargram that snow and overflow on the ice surface complicates measuring ice thickness using GPR, which is a major limitation of GPR when used by community members in Interior Alaska. Further, the regression plot in Fig. 6d indicates a weak correlation between measured ice thickness and average velocity model-calculated ice thickness under Condition 1, which produced the largest error of MAE = 10.6 cm (Table 2). These findings suggest that, though we removed the data points with overflow present from the dataset, snowpack conditions introduce the source of error and reduce GPR accuracy. Liquid water content of the snowpack affects relative dielectric permittivity. While we didn't measure liquid water content; presence of wet snow could explain higher error in ice thickness results collected for Condition 1.

An experiment to determine if the GPR signal (450 MHz) is impacted by the frazil ice at the ice-water interface, confirmed that the frazil ice accumulation does not obscure the bottom of the ice cover. There is a dielectric contrast between frazil ice and ice cover (Arcone et al., 1987) because the frazil ice deposits under the ice cover are saturated with water. Therefore, the radar return from the top of the frazil appears the same as the return from water itself. This finding is consistent with the literature on applicability of GPR for detecting frazil ice deposits (Arcone et al., 1987). Based on results from Annan and Davis (1977) that frazil ice could be detected with a 100 MHz antenna, it is likely that our frequencies used were too high to detect such an interface.

As presented in Table 2, a consistent wave velocity was calculated for each location and time. Regardless of antenna frequency, the same average wave velocity was calculated for both Trench Road transects and both Packed Road transects. The wave velocity calculated on the Tanana River is the same for 2019 and 2020, suggesting that the ice formed at this location was similar in structure and volumetric air content from 2019 to 2020, and any change in thickness did not greatly affect the velocity. However, the change in RMSE from 2019 to 2020 suggests that different snow conditions affect the accuracy of the GPR data. Error is most likely attributable to how uneven the snow cover is, as this affects the path of the radar pulse.

Finally, based on the results in Table 2, we found no correlation between the antenna frequency and the MAE or RMSE. A similar range of radar wave velocities, approximately 0.13–0.16 m/ns, has been reported in previous work (Annan et al., 2016). The wave velocities estimated in this study (0.156–0.170 m/ns) partially overlapped this range. The faster wave velocity on the Yukon River may be due to higher volumetric air content in that ice cover.

6.3. Common midpoint analysis

We used CMP analysis to verify if there was enough vertical contrast in velocity within the river ice to identify layers of ice with different densities. Our results show that the density variance in the river ice is not significant enough to be detected using 800 MHz antennas and the utilized processing methods. Based on the concept that radargram detail and signal quality increase as antenna frequency increases, it may be necessary to employ a higher frequency antenna to see differentiation between layers with small change in ice density. The quality of results is also based partially on the exactness of spacing used in the CMP data collection. The ice surface is very uneven on the Tanana River, and therefore the quality of data produced is not ideal. This issue with uneven ice cover may be resolvable with an antenna on the order of 2–10 GHz due to increased detail with higher frequency antennas (Marshall and Koh, 2008), or it may be necessary to design a stabilization system for the antenna so that an uneven ice surface does not affect the quality of data collected. This option may be feasible for the public using GPR systems if a low-cost piece of equipment is designed.

6.4. Limitations

The largest limitation experienced in GPR data collection is the complication of measuring ice thickness accurately in areas where snow with overflow is present. For Condition 1, the only condition with overflow and saturated snowpack present, overflow reduced the number of useable comparison points from 22 to 11. It can be clearly deduced that wet snow and overflow interfered with the radar in the middle portion of the Tanana River 2019 transect where there are instances of multiples (Fig. 6b). Practically, sections of floating ice roads with saturated snowpack and overflow would require additional instruments and methods for monitoring ice thickness. GPR determination of ice thickness is still possible when surface liquid water is present (Arcone, 1991), but it would likely require a lower frequency GPR (depending on amount of liquid water present). If there is a very thin layer of surface water (<8 mm) and ice surface is relatively smooth, the ice thickness can still be interpreted with a center frequency of 500 MHz using plane-wave theory (Arcone, 1991).

The zero-offset assumption used in the GPR distance and velocity calculations is a limitation on the thin non-uniform ice cover. As mentioned earlier, the zero-offset assumption is acceptable when the distance between transmitting and receiving antennae is considerably smaller than the ice thickness. For example, for 1 m of ice thickness, the zero-offset approach would generate an error of <0.5% on the ice radar velocity estimation. However, for ice thickness < 0.3 m, that would

generate a bias error in the ice radar velocity estimation.

Note that the presence of snow and cold temperatures tends to increase the difficulty of collecting high-quality data. On snow, the GPR wheel tends to slide rather than turn occasionally, which made it extremely important to place surface markers at our drilled measurement holes to avoid unnecessary dependence on the wheel-collected distances. For our research, GPS acquisition alone was used for distance calculations; however, this limitation should be considered in situations in which the wheel is the only available option due to limited positioning solutions.

Snow cover is identified as a factor contributing to the accuracy of ice thickness measurements using GPR. Calculating the snow density for transects with snow cover would be necessary to obtain accurate GPR ice thickness measurements. Snow density was not collected in 2019 and therefore an assumption was made for the dielectric permittivity of the snow cover which could have introduced error into our calculations. We noticed on the transects collected on the Yukon River Packed Road that pulling the GPR unit over an uneven snow surface may prevent the detection of the ice-water interface reflection. If the angle of the unit in relation to the ice cover is constantly changing abruptly (particularly when not perpendicular to the ice cover), the ice-water interface reflection may be missed due to high amounts of refraction.

6.5. *Further work: identifying ice types*

Rather than calculating velocity from common offset and manual ice thickness measurements, the velocity can also be estimated based on multi-offset GPR measurements (Parsekian, 2018). This method shows potential for future work to calculate velocity with greater accuracy, as well as in determining the dielectric permittivity. Additionally, using a higher frequency antenna, it may be possible to identify smaller differences in relative permittivity between various ice types. Identifying ice types could also be accomplished by 1) transmission lab tests using a transmitter and receiver to send a one-way radar pulse through various ice samples, or 2) measuring ice thickness and density in the lab to determine radar velocity, using a relationship that has previously been determined by Li et al. (2010). A more controlled lab environment may be beneficial for identifying these small differences in permittivity. Identifying various ice types is an important and useful undertaking because northern communities historically have used the Gold Formula (Saskatchewan Winter Roads Handbook, 2010), which requires knowledge of ice composition to design ice roads and calculate structural capacity.

Additionally, an important aspect of ice cover analysis using GPR could be to calculate the reflective strength of the signal at each interface. Reflective strength was analyzed only visually for this manuscript, and while calculating reflective strength falls outside the scope of this paper it would be useful for determining the most effective frequency for a given ice cover as well as expanding on why frazil ice could not be identified in our collected transections.

7. Conclusion

Ground penetrating radar was successfully and accurately used to measure ice thickness in 2 locations over 2 years in Interior Alaska. Average radar wave velocities through ice cover on the Tanana River, Yukon River Trench Road, and Yukon River Packed Road were determined to be 0.156 m/ns, 0.164 m/ns, and 0.170 m/ns, respectively. These values correspond well with the range of velocities calculated in previous GPR investigations on ice cover. We observed that overflow conditions complicate the ability to use GPR to accurately measure river ice thickness because most of the GPR signal is reflected on the wet snow-ice interface, which prevents the detection of the ice-water interface. However, based on a visual qualitative inspection, the presence of frazil ice does not appear to affect the quality of GPR data AND is not identifiable in the radargrams. It is clear from the variance in RMSE and MAE between the three conditions that snow cover and overflow can affect the accuracy of using a constant radar velocity model. While the radargrams collected in this analysis do not appear to show interfaces between the different types of ice (primary, secondary, and superimposed), applying a higher frequency antenna could allow identification of these interfaces. We found that, overall, GPR excels at river ice measurement in certain conditions and can be used to improve our understanding of ice cover on remote high-latitude river ice roads. Understanding the effect of environmental conditions (such as the presence of snow, rough ice surface, or other ice conditions) on measuring ice thickness accurately with GPR is of special importance, especially for remote communities in rural Alaska. In these locations where ice roads are used regularly as winter transportation routes, accurate measurements are crucial to calculating allowable loads for transporting heavy equipment on the ice cover, thereby decreasing property damage or loss and increasing the safety of community members.

Data and materials availability

Data associated with this research are available at the Harvard Dataverse (Richards and Stuefer, 2021).

CRediT authorship contribution statement

Elizabeth Richards: Data curation, Formal analysis, Investigation, Methodology, Software, Validation, Visualization, Writing – original draft. **Svetlana Stuefer:** Conceptualization, Funding acquisition, Writing – original draft. **Rodrigo Correa Rangel:** Formal analysis, Data curation, Investigation, Methodology, Software, Writing – original draft. **Christopher Maio:** Conceptualization, Data curation, Writing – original draft. **Nathan Belz:** Conceptualization, Data curation, Writing – original draft. **Ronald Daanen:** Conceptualization, Data curation, Writing – original draft.

Declaration of Competing Interest

None.

Data availability

Data are available through the Harvard Dataverse (Richards and Stuefer, 2021).

Acknowledgements

This work was supported by funding from the Pacific Northwest Transportation Consortium award number 69A3551747110 and by the U.S. Department of Transportation University Transportation Center program, award number 69A3551747129 through the Center for Safety Equity in Transportation. We would like to thank two reviewers for providing comments and suggestions on earlier version of this manuscript.

References

Annan, A.P., Davis, J.L., 1977. Impulse radar applied to ice thickness measurements and freshwater bathymetry. Report Activ. Part B. Geol. Surv. Canada 77, 63–65.

Annan, A.P., Diamanti, N., Redman, J.D., Jackson, S.R., 2016. Ground-penetrating radar for assessing winter roads. Geophysics 81. https://doi.org/10.1190/GEO2015-0138.1. WA101–109.

Arcone, S.A., 1991. Dielectric constant and layer-thickness interpretation of helicopter-borne short-pulse radar waveforms reflected from wet and dry river-ice sheets. IEEE Trans. Geosci. Remote Sens. 29 (5), 768–777.

Arcone, S.A., Brockett, B.E., Lawson, D.E., Chacho, E.F., 1987. Evaluation of the magnetic induction conductivity method for detecting frazil ice deposits. CRREL Report 87-17, 19.

Ashton, G.D., 1986. River and Lake Ice Engineering. Water Resources Publications.

Ashton, G.D., 2011. River and lake ice thickening, thinning, and snow ice formation. Cold Reg. Sci. Technol. 68 https://doi.org/10.1016/j.coldregions.2011.05.004, 1–2, 3–19.
Beltaos, S., 2013. River Ice Formation: Committee on River Ice Processes and the Environment. Canadian Geophysical Union Hydrology Section.
Belz, N., Chang, K., 2018. Mixed-Use Safety on Rural Facilities in the pacific Northwest. Pacific Northwest Transportation Consortium.
Brandt, O., Langley, K., Kohler, J., Hamran, S.-E., 2007. Detection of buried ice and sediment layers in permafrost using multi-frequency ground penetrating radar: a case examination on Svalbard. Remote Sens. Environ. 111, 212–227. https://doi.org/10.1016/j.rse.2007.03.025.
Daly, S.F., 2013. Chapter 4: Frazil Ice *in* Beltaos, S., River Ice Formation: Committee on River Ice Processes and the Environment. Canadian Geophysical Union, Hydrology Section, pp. 107–134.
Daniels, J.J., 2000. Ground Penetrating Radar Fundamentals. U.S. Environmental Protection Agency.
Dibike, Y., Prowse, T., Saloranta, T., Ahmed, R., 2011. Response of northern hemisphere lake-ice cover and lake-water thermal structure patterns to a changing climate. Hydrol. Process. 25, 2942–2953. https://doi.org/10.1002/hyp.8068.
Ensome, T., Morse, P., Kane, D., Alekseev, V., Marsh, P., 2020. The distribution and dynamics of aufeis in permafrost regions. Permafr. Periglac. Process. 1–13 https://doi.org/10.1002/ppp.2051.
Finlay, P.I., Parry, N., Proskin, S., Mickle, R., 2008. An overview of ice profiling using ground penetrating radar (GPR). In: Environmental and Engineering Geophysical Society - 21st Symposium on the Application of Geophysics to Engineering and Environmental Problems 2008.
Fu, H., Liu, Z., Guo, X., Cui, H., 2018. Double-frequency ground penetrating radar for measurement of ice thickness and water depth in rivers and canals: Development, verification and application. Cold Reg. Sci. Technol. 154, 85–94. https://doi.org/10.1016/j.coldregions.2018.06.017.
Galley, R.J., Trachtenberg, M., Langlois, A., Barber, D.G., Shafai, L., 2009. Observations of geophysical and dielectric properties and ground penetrating radar signatures for discrimination of snow, sea ice and freshwater ice thickness. Cold Reg. Sci. Technol. 57, 29–38. https://doi.org/10.1016/j.coldregions.2009.01.003.
Goldsmith, S., 1990. Understanding Alaska's Remote Rural Economy. University of Alaska Research Summary (No. 10).
Gow, A.J., 1986. Orientation textures in ice sheets of quietly frozen lakes. J. Cryst. Growth 74, 247–258. https://doi.org/10.1016/0022-0248(86)90114-4.
Hicks, F.E., 2016. An Introduction to River Ice Engineering for Civil Engineers and Geoscientists. CreateSpace Independent Publishing Platform.
Kämäri, M., Alho, P., Colpaert, A., Lotsari, E., 2017. Spatial variation of river-ice thickness in a meandering river. Cold Reg. Sci. Technol. 137, 17–29. https://doi.org/10.1016/j.coldregions.2017.01.009.
Kiani, S., Irannezhad, M., Ronkanen, A.K., Moradkhani, H., Kløve, B., 2018. Effects of recent temperature variability and warming on the Oulu-Hailuoto ice road season in the Northern Baltic Sea. Cold Reg. Sci. Technol. 151, 1–8. https://doi.org/10.1016/j.coldregions.2018.02.010.
Li, Z.J., Jia, Q., Zhang, B.S., Leppäranta, M., Lu, P., Huang, W.F., 2010. Influences of gas bubble and ice density on ice thickness measurement by GPR. Appl. Geophys. 7, 105–113. https://doi.org/10.1007/s11770-010-0234-4.
Liu, H., Xie, X., Sato, M., 2013. New Ground Penetrating Radar System for Quantitative Characterization of Snow and Sea Ice, 1–5. IET Conference Publications.
Maijala, P., Moore, J.C., Hjelt, S.-E., Palli, A., Sinisalo, A., 1998. GPR Investigations of Glaciers and Sea Ice in the Scandinavian Arctic: Proceedings of the 7th International Conference on Ground Penetrating Radar (GPR'98), pp. 27–30.
Marko, J.R., Jasek, M., 2008. Acoustic detection and study of frazil ice in a freezing river during the 2004-2005 and 2005-2006 winters. In: Proceedings of the 19th IAHR International Symposium on Ice: using New Technology to Understand Water-Ice Interaction. International Association of Hydraulic Engineering and Research, pp. 449–461.
Marshall, H.P., Koh, G., 2008. FMCW radars for snow research. Cold Reg. Sci. Technol. 52, 118–131. https://doi.org/10.1016/j.coldregions.2007.04.008.
Michel, B., Ramseier, R.O., 1971. Classification of river and lake ice. Can. Geotech. J. 8, 36–45. https://doi.org/10.1139/t71-004.
Mullan, D., Swindles, G., Patterson, T., Galloway, J., Macumber, A., Falck, H., Crossley, L., Chen, J., Pisaric, M., 2017. Climate change and the long-term viability of the world's busiest heavy haul ice road. Theor. Appl. Climatol. 1089–1108. https://doi.org/10.1007/s00704-016-1830-x.
Nakanishi, A.S., Dorava, J.M., 1994. Overview of Environmental and Hydrogeologic Conditions at Galena. United States Geological Survey, Alaska.
Neal, A., 2004. Ground-penetrating radar and its use in sedimentology: Principles, problems and progress. Earth Sci. Rev. 66, 261–330. https://doi.org/10.1016/j.earscirev.2004.01.004.
Olhoeft, G.R., 1998. Electrical, magnetic, and geometric properties that determine ground penetrating radar performance. In: Proceedings of GPR'98, Seventh International Conference on Ground Penetrating Radar, pp. 177–182.
O'Neill, K., Arcone, S.A., 1991. Investigations of Freshwater and Ice Surveying using Short-pulse radar: CRREL Report, 91-15. https://doi.org/10.1017/CBO9781107415324.004.
Osborne, E., Richter-Menge, J., Jeffries, M., 2018. Arctic Report Card 2018: Effects of Persistent Arctic Warming Continue to Mount: Arctic Report Card 2018. www.arctic.noaa.gov/Report-Card.
Osterkamp, T.E., Gosink, J.P., 1983. Frazil ice formation and ice cover development in interior Alaska streams. Cold Reg. Sci. Technol. 8, 43–56. https://doi.org/10.1016/0165-232X(83)90016-2.
Parsekian, A.D., 2018. Inverse methods to improve accuracy of water content estimates from multi-offset GPR. J. Environ. Eng. Geophys. 23, 349–361. https://doi.org/10.2113/JEEG23.3.349.
Proskin, S.A., Parry, N.S., Finlay, P., 2011. Applying GPR in assessing the ice bridges, ice roads and ice platforms. In: Committee on River Ice Processes and the Environment. In: http://cripe.ca/docs/proceedings/16/Proskin-et-al-2011.pdf.Richards.
Richards, E., Stuefer, S., 2021. Ice Thickness Measurements using Manual and GPR Methods on the Tanana and Yukon Rivers in Iinterior Alaska, V1. Harvard Dataverse. https://doi.org/10.7910/DVN/ZIOZAY.
Saskatchewan Winter Roads Handbook, 2010. Safe Operating Procedures for Winter Roads Committee (SOPWRC). Winter Roads Handbook. Saskatchewan Ministry of Highways and Infrastructure, Saskatoon.
Schneider, W., Brewster, K., Keilland, K., Jones, C., 2013. In: Elmer, E. (Ed.), On Dangerous Ice: Changing Ice Conditions on the Tanana River: The Oral History Program. Ramuson Library and the Institute of Arctic Biology University of Alaska Fairbanks.
Stephenson, S., 2012. The role of winter/ice roads in industry and communities in northern Alberta. In: Proceedings from the First International Conference on Urbanisation in the Arctic, 1, pp. 67–72.
Stuefer, S., Richards, E.M., 2021. River Ice Measurements for Transportation Safety in Rural Communities. Final Project Report. Pacific Northwest Transportation Consortium.
Stuefer, S., Kane, D.L., Dean, K.M., 2020. Snow water equivalent measurements in remote arctic Alaska watersheds. Water Resour. Res. 56.
Zhi-Jun, L., Qing, J., Bao-Sen, Z., Matti, L., Peng, L., Wen-Feng, H., 2010. Influences of gas bubble and ice density on ice thickness measurement by GPR. Appl. Geophys. 7, 105–113. https://doi.org/10.1007/s11770-010-0234-4.